

Intelligent Collaborative Optimization for Rubber Tyre Film Production Based on Multi-path Differentiated Clipping Proximal Policy Optimization

Yinghao Ruan, Wei Pang, Shuaihao Liu, Huili Yang, Leyi Han, Xinghui Dong, *Member, IEEE*

Abstract—The advent of smart manufacturing is addressing the limitations of traditional centralized scheduling and inflexible production line configurations in the rubber tyre industry, especially in terms of coping with dynamic production demands. Contemporary tyre manufacturing systems form complex networks of tightly coupled subsystems pronounced nonlinear interactions and emergent dynamics. This complexity renders the effective coordination of multiple subsystems, posing an essential yet formidable task. For high-dimensional, multi-objective optimization problems in this domain, we introduce a deep reinforcement learning algorithm: Multi-path Differentiated Clipping Proximal Policy Optimization (MPD-PPO). This algorithm employs a multi-branch policy architecture with differentiated gradient clipping constraints to ensure stable and efficient high-dimensional policy updates. Validated through experiments on width and thickness control in rubber tyre film production, MPD-PPO demonstrates substantial improvements in both tuning accuracy and operational efficiency. The framework successfully tackles key challenges, including high dimensionality, multi-objective trade-offs, and dynamic adaptation, thus delivering enhanced performance and production stability for real-time industrial deployment in tyre manufacturing.

Index Terms—Deep Learning, Intelligent Coordination, Proximal Policy Optimization Algorithm (PPO), Reinforcement Learning, Rubber tyre Manufacturing

I. INTRODUCTION

UNDER the global trend of intelligent manufacturing transformation, the rapid development of smart manufacturing and Industry 4.0 has promoted the evolution of process industries into intelligent and networked architectures [1]. Rubber tyre production, as a representative process industry, exhibits characteristics such as complex process flows,

This study was supported by the National Key Research and Development Program of China (No. 2022YFB3305300). (Corresponding author: Xinghui Dong).

Y. Ruan, S. Liu, and X. Dong are with the State Key Laboratory of Physical Oceanography and the Faculty of Information Science and Engineering, Ocean University of China, Qingdao, 266100. Y. Ruan is with the Faculty of Information Science and Engineering, Ocean University of China, Qingdao, 266100. W. Pang are with the School of Mathematical and Computer Sciences, Heriot-Watt University, Edinburgh, EH14 4AS. H. Yang is a Senior Engineer (Principal) at Mesnac Co., Ltd. L. Han is an Associate Senior Engineer at Mesnac Co., Ltd. (e-mail: ruan.yinghao@stu.ouc.edu.cn, lsh7117@stu.ouc.edu.cn, xinghui.dong@ouc.edu.cn, w.pang@hw.ac.uk, yanghl@mesnac.com, hanly@mesnac.com).

strongly coupled parameters, and high-precision quality control requirements. Specifically, tyre manufacturing involves multiple critical stages including mixing, calendaring, tyre building, and vulcanization, each requiring coordinated control of multiple variables, such as temperature, pressure, and speed. Taking the tread calendaring process as an example, the control precision of width and thickness directly affects the uniformity and durability of finished tyres.

The optimization of rubber tyre film production holds significant implications for enhancing product quality, reducing production costs, and advancing green manufacturing. Firstly, precise dimensional control of the film is fundamental to ensuring structural integrity and driving safety of tyres, directly influencing their dynamic balance and wear performance. Secondly, coordinated parameter optimization during production can significantly reduce material waste and energy consumption, aligning with sustainable development goals. Furthermore, the introduction of intelligent optimization methods facilitates the development of adaptive and scalable production systems, promoting the transition of the tyre industry toward digitalized and flexible manufacturing paradigms. This provides a technical framework for the intelligent transformation of process industries.

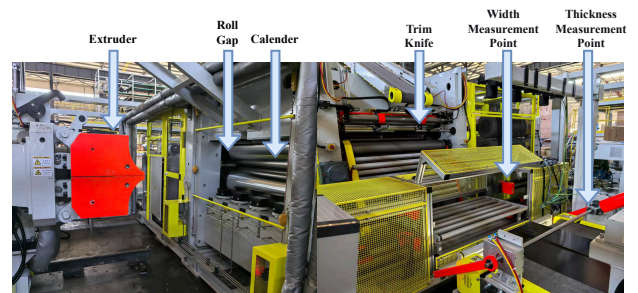


Fig. 1: Rubber Tyre Film Manufacturing Equipment.

Traditional control methods face challenges in achieving dynamic coordination and global optimization across industrial processes. In complex multi-stage production systems, there are implementations that leverage the integration of IoT [2], digital twins [3], multi-agent systems (MAS) [4], and deep reinforcement learning (DRL) [5], demonstrating potential in enhancing overall synergistic efficiency and achieving dynamic optimization.

Digital twins facilitate real-time mapping of physical systems, supporting parameter optimization and anomaly diagnosis, while DRL techniques, including Proximal Policy Optimization (PPO) [6] and Twin Delayed Deep Deterministic Policy Gradient (TD3) [7], have shown strong performance in continuous control and collaborative optimization. Additionally, Transformer and graph neural networks (GNNs) enhance high-dimensional state representation and cross-domain generalization. Nevertheless, tyre production remains a challenging domain due to its high dimensionality, strong coupling, and nonlinear dynamics, demanding more robust and adaptive collaborative algorithms.

Proximal Policy Optimization (PPO), while valued for its stability in industrial control, exhibits limitations in high-dimensional state-action spaces which is typical in tyre production. Its fixed clipping mechanism proves inadequate under dynamic operating conditions, leading to optimization instability, while difficulties in balancing exploration-exploitation and sensitivity to reward design further constrain its effectiveness in collaborative optimization tasks.

To overcome these challenges, this study introduces a multi-path differentiated clipping mechanism that enables dimension-aware policy updates. The enhanced algorithm demonstrates accelerated convergence, improved stability in dynamic environments, enhanced multi-objective optimization capability, and greater robustness, thus offering a more reliable control solution for rubber tyre manufacturing.

The main contributions of this work are listed as follows:

- We propose an autonomous optimization framework integrating deep learning and reinforcement learning to achieve dynamic perception, quality prediction, and self-adaptive parameter control in industrial processes.
- We introduce a predict model that effectively captures both short-term local dependencies and long-term trends in multi-dimensional process parameters.
- We develop a Multi-path Differentiated Clipping Proximal Policy Optimization (MPD-PPO) algorithm, employing a multi-path policy network and differentiated clipping mechanism to enhance training stability and optimization efficiency in high-dimensional action spaces.
- We design a composite reward function for rubber tyre film production, incorporating exponential decay and hyperbolic tangent components to balance quality accuracy, operational stability, and energy efficiency in multi-objective optimization.

The remainder of this paper is structured as follows. Section II reviews related work in industrial reinforcement learning and predictive modeling. Section III introduces the proposed methodology, including the LSTNet predictive model and the MPD-PPO algorithm with its multi-path architecture. Section IV presents experimental results and analysis on rubber tyre film production. Finally, Section V concludes the paper and discusses future directions.

II. RELATED WORK

A. Deep Learning for Industrial Prediction

Deep learning has revolutionized industrial predictive capabilities by overcoming the limitations of traditional feature

engineering. Through successive architectural innovations, it has addressed diverse challenges in industrial data processing.

In industrial image processing, Convolutional Neural Networks (CNNs) [8] are widely applied in tasks such as surface defect detection and target positioning. Evolving from LeNet [9] to AlexNet [10], ResNet [11], and DenseNet [12], these architectures have significantly advanced feature extraction for visual inspection. Lightweight networks like MobileNet [13] and ShuffleNet [14] enable real-time edge applications, though with accuracy-efficiency trade-offs. Recently, Vision Transformers (ViT) [15] have demonstrated remarkable capabilities in capturing long-range dependencies, despite higher computational costs.

For temporal data processing, Recurrent Neural Networks (RNN) [16] and their variants dominate, with Long Short-Term Memory (LSTM) [17] and Gated Recurrent Units (GRU) [18] effectively capturing long-term dependencies, while Temporal Convolutional Networks (TCN) [19] and Transformers [20] offer advantages in parallel processing and complex pattern capture respectively, and graph neural networks (GNNs) [21] enhance high-dimensional state representation and cross domain generalization.

Despite these advancements, deep learning models primarily function as passive analyzers in industrial settings. While excelling at feature extraction and pattern recognition, they lack inherent capabilities for autonomous decision-making and action execution in dynamic environments.

B. Reinforcement Learning for Industrial Control

Reinforcement Learning (RL) has become a prominent framework for sequential decision-making in complex industrial environments, effectively tackling control and optimization problems beyond the reach of traditional methods.

The RL landscape includes several algorithm families tailored to industrial applications. Value-based methods such as Deep Q-Networks (DQN) [22] and its variants (Double DQN [23], Dueling DQN [24]) excel in discrete control tasks like production scheduling, yet are less suitable for continuous action spaces common in industrial systems.

Policy-based methods overcome this by directly optimizing parameterized policies. While REINFORCE offers a foundational approach, advanced algorithms like Trust Region Policy Optimization (TRPO) [25] and Proximal Policy Optimization (PPO) [6] ensure training stability, which is essential for safety-sensitive industrial settings. PPO, in particular, is widely adopted due to its clipped objective and robust performance.

Actor-critic methods merge value and policy-based advantages, proving effective for complex industrial tasks. Deep Deterministic Policy Gradient (DDPG) [26] extends DQN to continuous domains, enabling applications in robotic and process control. Twin Delayed DDPG (TD3) [7] enhances robustness via clipped double Q-learning and delayed updates, while Soft Actor-Critic (SAC) [27] promotes exploration through entropy maximization.

Multi-Agent RL (MARL) [28] methods address collaborative industrial systems. Algorithms such as VDN [29] and QMIX [30] solve credit assignment in multi-agent settings,

facilitating coordination in applications like automated logistics and smart energy grids.

Model-based RL (MBRL) [31] and Offline RL [32] offer improved sample efficiency through internal simulation and effective utilization of historical datasets, supporting multi-scale decision-making and reducing retraining needs.

Despite the above mentioned advances, key challenges remain. RL algorithms are often sample-inefficient, requiring large amounts of costly or risky operational data. Reward design lacks systematic methodology, and safety during exploration remains a critical barrier-especially in real-world industrial deployments.

III. A PREDICTIVE-OPTIMIZATION CLOSED LOOP METHOD FOR INDUSTRIAL CONTROL

Modern industrial processes like tyre manufacturing exhibit strongly-coupled parameters across stages, making multi-objective optimization essential yet challenging. This paper proposes an integrated LSTNet and MPD-PPO framework to overcome suboptimal sequential methods. LSTNet captures temporal dependencies for quality prediction, while MPD-PPO’s multi-branch policy enables parallel objective optimization, achieving adaptive decision-making under complex constraints control precision and system efficiency in dynamic industrial environments.

A. Overview

The workflow of the collaborative optimization method integrating LSTNet and MPD-PPO for industrial control is illustrated in Fig. 2. The initialization phase involves constructing an MPD-PPO agent, which consists of an actor network with N independent pathways and a shared critic network. Each action pathway’s architecture is individually configurable and tailored to the physical properties of its specific actuator. For continuous action spaces, a trainable standard deviation parameter is assigned to each pathway, with its initial value determined by the actuator’s precision requirements. Before training commences, an experience replay buffer is initialized using a partitioned storage strategy, which maintains separate historical action probability distributions for every action pathway.

At each training timestep t , the environmental state s_t is fed into the policy network. Each action pathway then operates in parallel: shared network layers first extract foundational features, which are then processed by pathway-specific fully connected layers to produce the action mean values. Subsequently, actions a_t are stochastically sampled using the current standard deviation.

The outputs from all pathways are concatenated to form the final action vector a_t . The interaction with the environment then proceeds as follows: firstly, the environment decodes the continuous action vector a_t and reconstructs the input features for the downstream forecasting module. This is achieved by mapping action values to incremental set-points of process parameters, which accordingly alters the original data to generate a new time-series sample. This sample is then fed into the LSTNet network to acquire the next-step estimates

of parameters. Finally, the prediction error is normalized, and this normalized error serves as an instantaneous reward signal and is also used to form the subsequent state vector s_{t+1} .

The resulting transition tuple is stored in the experience replay buffer. The policy update phase is triggered as soon as the number of accumulated trajectories exceeds a predefined threshold. This ”interaction-prediction-reward-storage-update” loop iterates continuously until the policy converges to an equilibrium state, thereby achieving high-precision cooperative optimization of multiple process parameters.

B. A Deep Learning Framework for Industrial Prediction

Deep learning models offer strong predictive power and latent pattern identification in complex data. For time series prediction, architectures such as CNNs, LSTMs, and self-attention mechanisms are commonly chosen for their ability to capture temporal dynamics and long-range dependencies, with selection considering adaptability, learning efficiency, and computational complexity.

1) *Architecture for LSTNet*: As shown in Fig. 2, the proposed LSTNet integrates CNNs, LSTM, and a Skip-GRU module to concurrently capture multi-scale temporal patterns in industrial data. Utilizing a sliding window approach, it processes input sequences for localized feature extraction while preserving long-term temporal dependencies.

2) *Hierarchical Feature Extraction Pipeline*: The network employs a hierarchical feature extraction process, beginning with stacked 1D convolutional and pooling layers to capture multi-scale local patterns. The resulting features are then modeled for long-term dependencies by a unidirectional LSTM. Layer normalization and dropout are integrated throughout to ensure stable training and prevent overfitting.

3) *Skip-GRU Module for Multi-Scale Temporal Modeling*: In tyre manufacturing, a novel model integrates an LSTM pathway with a dedicated Skip-GRU module. The Skip-GRU captures multi-scale periodic patterns via skip-connected windows, while the LSTM models sequential dynamics. Their combined outputs are fused to comprehensively represent temporal dependencies, enabling accurate production prediction.

In summary, LSTNet effectively combines convolutional feature extraction, recurrent temporal modeling, and multi-scale skip connections to handle complex time series data, capturing both short-term fluctuations and long-term trends.

C. Multi-path Differentiated Clipping Proximal Policy Optimization

This study proposes an enhanced reinforcement learning algorithm named Multi-path Differentiated Clipping Proximal Policy Optimization (MPD-PPO), tailored for collaborative optimization in industrial processes. Building upon the Proximal Policy Optimization (PPO) framework, MPD-PPO introduces a multi-branch policy network architecture to address the limitations of uniform policy updates in traditional PPO when applied to industrial control. Each actuator corresponds to an independent policy branch, with the action distribution for the i -th actuator defined as follows:

$$\pi_{\theta_i}(a_i, s) = N(\mu_i(s), \sigma_i^2). \quad (1)$$

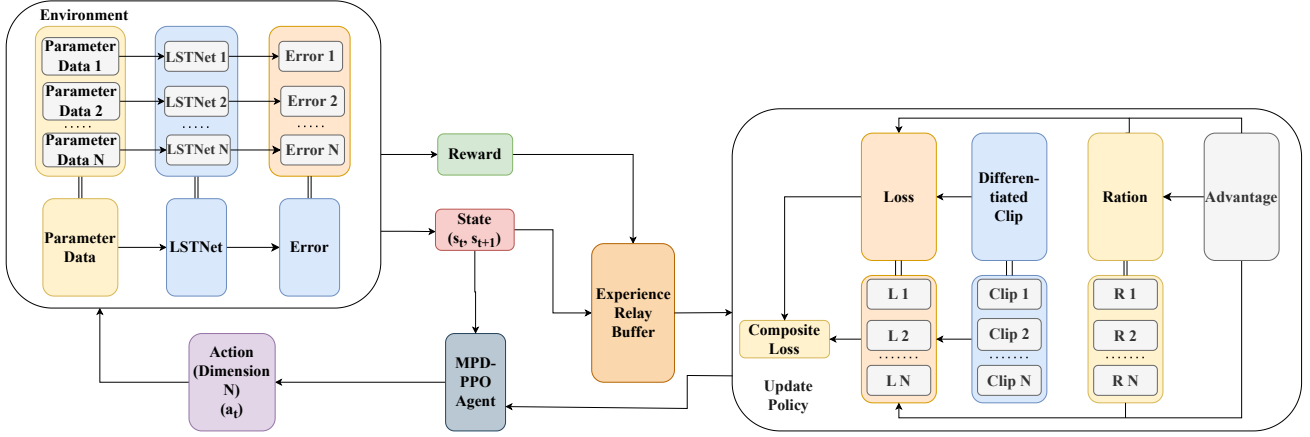


Fig. 2: The Workflow Diagram Of The Predictive-Optimization Closed Loop Method.

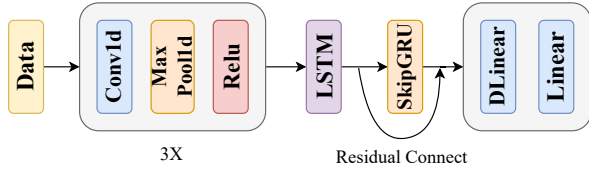


Fig. 3: Architecture of the LSTNet Model.

In the policy representation, the meaning of each variable is as follows: $\pi_{\theta_i}(a_i, s)$: probability distribution of action a_i given state s for the i -th actuator; θ_i : trainable parameters of the policy network corresponding to the i -th actuator; a_i : continuous action output of the i -th actuator; s : global environmental state; $\mu_i(s)$: state-dependent mean action generated by the neural network; σ_i^2 : variance controlling the exploration magnitude.

A key innovation of MPD-PPO is the differentiated Clip mechanism, which adaptively constrains policy updates per actuator based on dynamic response characteristics. The objective function for each path is formulated as follows:

$$L_i^{CLIP} = E_t[\min(r_t^i(\theta_i)A_t, \text{clip}(1 - \epsilon_i, 1 + \epsilon_i)A_t)], \quad (2)$$

where the importance sampling ratio $r_t^i(\theta_i) = \frac{\pi_{\theta_i}(a_t^i, s_t^i)}{\pi_{\theta_i, old}(a_t^i, s_t^i)}$ and the clipping threshold ϵ_i are configured dynamically.

The advantage function calculation employs pathway-specific discounted return estimation. For the i -th action pathway, the advantage estimate is given as follows:

$$A_i^t = G_i^t - V_i(s_t), \quad (3)$$

where the value function V_i is generated by the shared Critic network, G_i^t employs generalized advantage estimator (GAE) [33] for computation. This design enables different action pathways to adopt distinct discount factors γ_i according to their response characteristics.

Policy optimization begins by calculating and standardizing the Monte Carlo discounted returns. Following this, these returns are combined with the state-values from the current policy to compute advantage estimates, which drive the gradient update.

Within the updating loop, empirical data is reshuffled and partitioned into mini-batches. For each batch, a forward pass is conducted to compute the importance ratios for each action branch. To respect the distinct dynamics of individual process parameters, branch-specific clipping ranges are applied, and the resulting surrogate losses are weighted according to real-time control priorities (specified by weights w_i). The total loss function L_t combines the weighted surrogate loss, the value function loss (with coefficient c_1), and an entropy regularization term (with coefficient c_2). This loss is optimized via backpropagation with gradient accumulation, after which the policy parameters are updated, and the old policy is synchronized for the subsequent data collection phase. The update procedure of MPD-PPO is presented in Algorithm 1.

D. Reward Function

This study employs a composite reward function where individually computed objective-specific rewards are normalized and aggregated. This ensures balanced optimization across objectives with divergent numerical scales, promoting stable training.

1) *Error Reward*: an exponential decay function is employed to increase sensitivity to small errors and promote continuous precision improvement:

$$R_e = 2.0 \cdot \exp(-e_t). \quad (4)$$

2) *Progress Reward*: To maintain gradient stability and ensure the agent receives sustained incentives while enabling smooth and stable policy optimization, the hyperbolic tangent function constrains the reward values within the interval $(-0.3, 0.3)$, thereby motivating the agent to surpass historical performance benchmarks:

$$R_p = 0.3 \cdot \tanh(e_{\text{best}} - e_t). \quad (5)$$

3) *Action Penalty*: this term penalizes large adjustments in process parameters to encourage smooth control operations:

$$P_a = -0.05 \cdot (a_t - a_{t-1})^2. \quad (6)$$

Algorithm 1 MPD-PPO Update Policy

Require: Learning rate α , discount factor γ , epochs K , clip ranges ϵ_i , batch size B

Ensure: Optimized policy networks $\{\pi_{\theta_i}\}_{i=1}^N$

- 1: Initialize policy networks $\{\pi_{\theta_i}\}_{i=1}^N$, value network V_ϕ , optimizer
- 2: Initialize experience replay buffer \mathcal{B}
- 3: **for** each training episode **do**
- 4: Collect trajectory $\tau = \{(s_t, a_t, r_t, s_{t+1})\}$ and store in \mathcal{B}
- 5: **if** \mathcal{B} reaches predefined size **then**
- 6: Compute discounted returns: $R_t = \sum_{k=0}^{\infty} \gamma^k r_{t+k}$
- 7: Compute advantages: $A_t = R_t - V_\phi(s_t)$
- 8: **for** $k = 1$ **to** K **do**
- 9: Sample random batch: $\mathcal{B}_{batch} \sim \mathcal{B}$
- 10: **for** each policy network π_{θ_i} **do**
- 11: Compute probability ratio: $\rho_i(\theta) = \frac{\pi_{\theta_i}(a_t|s_t)}{\pi_{\theta_i,old}(a_t|s_t)}$
- 12: Compute clipped loss: $L_i^{CLIP} = \mathbb{E}[\min(\rho_i(\theta)A_t, \text{clip}(\rho_i(\theta), 1 - \epsilon_i, 1 + \epsilon_i)A_t)]$
- 13: **end for**
- 14: Compute value loss: $L^{VF} = \mathbb{E}[(V_\phi(s_t) - R_t)^2]$
- 15: Compute entropy bonus: $L^{ENT} = \mathbb{E}[H(\pi_\theta(s_t))]$
- 16: Total loss: $L^{TOTAL} = \sum_{i=1}^N w_i L_i^{CLIP} + c_1 L^{VF} + c_2 L^{ENT}$
- 17: Gradient update: $\theta \leftarrow \theta - \alpha \nabla_\theta L^{TOTAL}$
- 18: **end for**
- 19: Clear buffer \mathcal{B}
- 20: **end if**
- 21: **end for**

4) *Steady-State Reward*: this term provides incremental positive feedback when the system operates near the target value, thereby enhancing operational stability:

$$R_s = 0.5 \cdot (\tau - e_t). \quad (7)$$

The variables used in the above equations are defined as follows:

- e_t : the absolute tracking error at time step t , defined as $|y_t - y_{\text{target}}|$, where y_t is the current predicted value (e.g., width or thickness) and y_{target} is the desired value.
- e_{best} : the minimum observed tracking error throughout the current training episode.
- a_t : the current value of the adjusted process parameter (e.g., blade gap or roller distance).
- a_{t-1} : the previous value of the process parameter, used to compute the control action magnitude.
- τ : a constant threshold that defines the tolerance range for the steady-state region.

The overall reward at each time step is computed as the sum of these components:

$$R_t = R_e + R_p + P_a + R_s. \quad (8)$$

The reward coefficients were calibrated through sensitivity analysis to ensure balanced collaborative optimization, with total rewards clipped to a predefined range for numerical

stability during training. This structured reward design effectively integrates tracking precision, behavioral smoothness, and steady-state performance, addressing critical requirements of industrial control systems.

E. Simulation Environment for Industrial Collaborative Optimization

This study develops a high-fidelity simulation environment that serves as the core interface for reinforcement learning agents to interact with a simulated industrial production system. Tailored for collaborative optimization, the environment features a continuous, multi-dimensional action space for fine-grained parameter control and a state representation that captures temporal dependencies of key process variables. A composite reward function enables the balance of competing objectives, with dynamically adjustable weights to prioritize goals in real-time. Episode termination is governed by achieving predefined precision thresholds across all target metrics, ensuring comprehensive optimization. Built on real production data with a modular architecture, the environment provides a robust testbed for developing and transferring effective control policies to real-world applications.

IV. PERFORMANCE VALIDATION FOR RUBBER TYRE FILM PRODUCTION

Based on the integrated deep learning and reinforcement learning framework, this section presents empirical validation in the rubber tyre film calendering process. This scenario exhibits strongly coupled and nonlinear control of film width and thickness - critical quality parameters that challenge conventional methods.

The study innovatively combines temporal prediction models with the MPD-PPO algorithm: the former captures complex parameter dependencies to predict quality indicators, while the latter dynamically adjusts control strategies for optimal parameters under multiple constraints. Comparative experiments targeting width (480mm/380mm) and thickness (3.0mm/2.2mm) objectives demonstrate MPD-PPO's convergence behavior and optimization efficacy. Results show robust performance across all targets, providing empirical support for industrial applications.

A. Data Acquisition

To thoroughly investigate the relationship between rubber film width and various machine/environmental parameters, real-world process data were collected from the inner-liner production line. MESNAC¹, a key strategic partner and major supplier of intelligent manufacturing systems to the global tyre industry, provided continuous *in-situ* measurements via industrial IoT sensors and monitoring devices. The company's strong R&D capabilities ensured the reliability and precision of the dataset used in this study. As illustrated in Fig. 1, the manufacturing process begins with compound plasticization in an extruder. The material is then discharged onto a conveyor and fed into a calender to form a continuous sheet.

¹<https://en.mesnac.com/>

This sheet is subsequently cropped to the required width by edge-trimming knives, drawn through pull rolls, and finally delivered to the take-off conveyor. Thermal expansion and contraction cause the width and thickness of the trimmed and drawn strip to fluctuate until the sheet stabilizes at the take-off section. A critical constraint arises from the equipment setup: width and thickness gauges are installed several meters downstream on the take-off belt, introducing a measurement delay. This delay not only prevents real-time monitoring of the current process state but also leads to material waste during product-specification changes. Consequently, the continuous process data collected from this line (Fig. 3) provide a valuable foundation for developing intelligent predictive models. According to plant engineers, film width and thickness are governed by the machine parameters listed in Tables I and II. By tuning these parameters, it is possible to achieve concurrent optimization of both width and thickness.

TABLE I: Key Factors Influencing the Width of Rubber Tyre Film.

Technical Parameter	Function
Main-motor current of calender (A)	/
Calender line-speed (mm)	/
Discharge temperature of calender ($^{\circ}C$)	/
Draw-roll speed of calender (mm)	/
Conveyor-belt speed (mm)	/
Actual knife-to-knife distance of edge-trimming unit (mm)	Control variable
Top-roll temperature of calender ($^{\circ}C$)	/
Bottom-roll temperature of calender ($^{\circ}C$)	/
Main-motor current of extruder (A)	/
Extruder screw speed (mm)	/
Extruder head pressure (N)	/
Extruder head temperature ($^{\circ}C$)	/
Extruder screw-tip pressure (N)	/
Extruder head temperature-control set-point ($^{\circ}C$)	/
Extruder plasticizing zone-1 temperature ($^{\circ}C$)	/
Extruder plasticizing zone-2 temperature ($^{\circ}C$)	/
Extruder barrel temperature ($^{\circ}C$)	/
Extruder screw temperature ($^{\circ}C$)	/

TABLE II: Key Factors Influencing the Thickness of Rubber Tyre Film.

Technical Parameter	Function
Extruder screw speed (mm)	/
Extruder main-motor current (A)	/
Extruder outlet temperature ($^{\circ}C$)	/
Extruder outlet pressure (N)	/
Extruder screw-tip pressure (N)	/
Screw temperature-control set-point ($^{\circ}C$)	/
Plasticizing zone-1 temperature ($^{\circ}C$)	/
Plasticizing zone-2 temperature ($^{\circ}C$)	/
Extruder head temperature ($^{\circ}C$)	/
Calender line-speed (mm)	/
Calender main-motor current (A)	/
Sheet temperature after calender ($^{\circ}C$)	/
DS (drive-side) roll gape (mm)	Control variable
OS (operator-side) roll gap (mm)	Control variable
Edge-trimming knife spacing (mm)	/
Prick-roll temperature ($^{\circ}C$)	/
Extrusion-section temperature ($^{\circ}C$)	/

B. Experimental Results Of Prediction

For width and thickness prediction, the LSTNet was trained using the Adam optimizer with Mean Absolute Error (MAE) as the loss function. We trained two separate prediction models on the collected width and thickness datasets, respectively. After 100 training epochs with a learning rate of 0.001 and a batch size of 1024, both models achieved convergence. Subsequent evaluation on the test set yielded the average prediction error and qualification rate, which are summarized in Table III. The qualification rate is defined as the proportion of samples whose prediction errors for both width and thickness are within the tolerance ranges specified by the factory (± 1 mm for width, ± 0.05 mm for thickness).

TABLE III: Predicted Results Of LSTNet for Width and Thickness.

Data	MAE (mm)	RMSE (mm)	Qualification Rate
Width	1.865 ± 0.099	2.458 ± 0.138	0.452 ± 0.073
Thickness	0.204 ± 0.053	0.316 ± 0.074	0.579 ± 0.024

To systematically assess the effectiveness and generalization of the proposed prediction model, this study conducts an empirical comparative analysis using tyre film width prediction as a representative production task. All models were trained under identical hyperparameters, including a learning rate of 0.001 and a batch size of 1, 024, and for 100 epochs per run, with results averaged over 10 independent trials. Four models were used for comparison, including BILSTM[34], Linear Regression (LR), TCN[19] and Informer[35]. The models were evaluated on four metrics: MAE, RMSE, and Qualification Rate (QR). The comparative experimental results are summarized in Table IV.

TABLE IV: A Comparative Study of Predictive Performance Between LSTNet and Other Networks.

Net	MAE (mm)	RMSE (mm)	QR
BILSTM [34]	19.125 ± 0.654	26.955 ± 1.006	0.097 ± 0.052
LR	3.782 ± 1.212	4.604 ± 1.449	0.206 ± 0.068
TCN [19]	10.188 ± 0.759	14.071 ± 1.094	0.129 ± 0.055
Informer 36	13.689 ± 0.872	19.551 ± 1.257	0.095 ± 0.018
LSTNet	1.865 ± 0.099	2.458 ± 0.138	0.452 ± 0.073

C. Experimental Results Of Optimization

The MPD-PPO algorithm utilizes separate policy networks for width and thickness adjustment, complemented by an adaptive clipping mechanism. This hierarchical architecture features shared layers for modeling global interactions and dedicated branches for process-specific optimization.

In the clipping mechanism design, MPD-PPO dynamically sets clipping thresholds based on parameter sensitivity analysis:

- Width control (larger-scale adjustments): we use a relaxed clipping threshold range of (0.8, 1.2)
- Thickness control (finer-scale adjustments): we employ a stricter clipping threshold range of (0.9, 1.1)

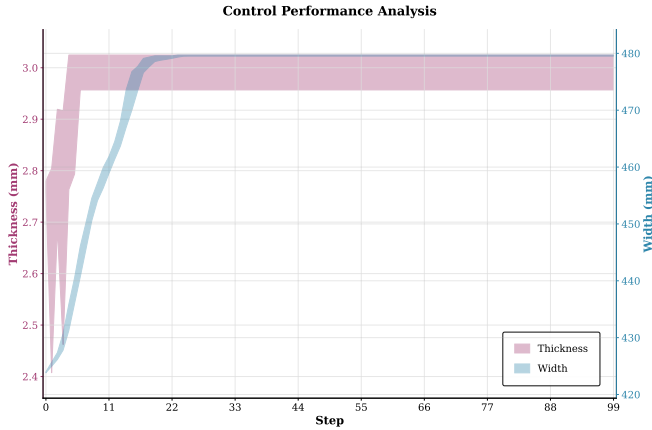


Fig. 4: MPD-PPO Optimization Performance at 50 Training Steps.

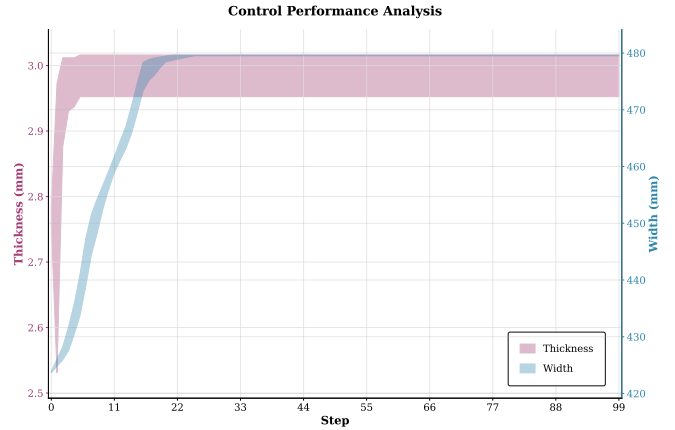


Fig. 5: MPD-PPO Optimization Performance at 100 Training Steps.

For width control, a looser clipping bound allows for larger-magnitude adjustments, whereas for thickness, a tighter bound prevents aggressive updates to ensure stable fine-tuning. This study investigates the impact of training steps per episode on the optimization performance of the MPD-PPO agent. We systematically compared configurations of 50 and 100 training steps per episode to evaluate their effects on convergence behavior and solution quality, where at each time step the agent selects an action. To enhance the robustness of the findings, we conducted five independent experimental trials and consolidated the resulting optimization curves into an intuitive interval representation for visualization. The experimental outcomes after 50 and 100 training episodes are presented in Fig. 4, Fig. 5, and Table V. It is noteworthy that the thickness curve appears wider post-convergence in the figure. This is a visual effect resulting from the high resolution of the y-axis scale, which is necessitated by its small absolute numerical range, rather than an indication of increased actual volatility.

TABLE V: Performance of the MPD-PPO Algorithm.

Train Step	Target (Width, Thickness) (mm)	Average Optimize Step
50	(480, 3.0)	23
	(480, 2.2)	18
	(380, 3.0)	14
	(380, 2.2)	19
100	(480, 3.0)	22
	(480, 2.2)	19
	(380, 3.0)	14
	(380, 2.2)	16

At 50 training steps, the optimization results demonstrate considerable effectiveness, though minor oscillations are observed in localized regions. By 100 training steps, the agent exhibits significantly improved performance, consistently achieving optimization targets within approximately 20 steps across all evaluated episodes. These results indicate robust convergence and high sample efficiency of the proposed method.

D. Ablation Study

This section evaluates the effectiveness of the multi-branch network architecture and the proposed differential clipping strategy against two baseline methods: PPO and MPD-PPO. During agent training, a consistent protocol was used, with each agent trained for 100 episodes, each comprising 100 time steps.

1) *The Influence Of Multi-Branch Network:* In this experiment, we replaced the original single-network architecture of the PPO algorithm with a two-branch network, comprising separate width and thickness action networks to investigate the efficacy of the branched architecture. Representative results for the typical operating condition of 480 mm width and 3.0 mm thickness are presented for comparative analysis. Table VI summarizes the quantitative results. Figures 6 and 7 present the performance of PPO with Multi-Branch Network and standard PPO, respectively, following the MPD-PPO results in Fig 5.

Based on the experimental results, replacing the original policy network with a dual-branch architecture yields significant performance improvements. Although the width optimization still does not reach the target value, its deviation is substantially reduced compared to conventional PPO. Furthermore, both width and thickness optimization trajectories demonstrate smoother profiles relative to the traditional approach.

TABLE VI: Optimization Results Of Removing Differentiated Clip.

Algorithm	Average Optimize Step
MPD-PPO	22
PPO With Multi-Branch Network	100 (Failed)
PPO	100 (Failed)

2) *The influence of Differentiated Clipping:* This experiment sets identical clipping thresholds for both branches to investigate the efficacy of the differentiated clipping strategy. Representative results for a width of 480 mm and a thickness of 3.0 mm are presented for comparative analysis. The corresponding quantitative results are summarized in Table VII.

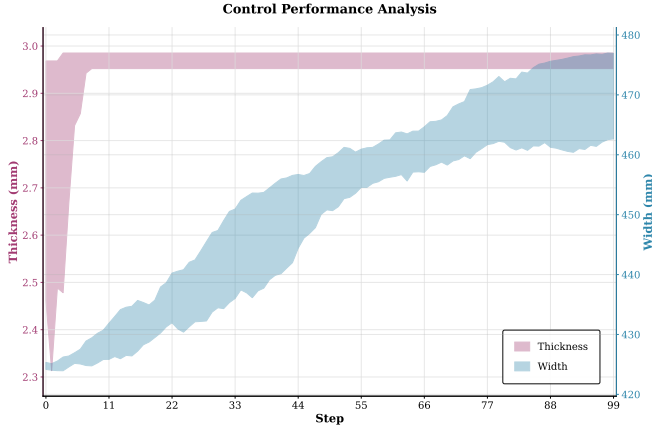


Fig. 6: Optimization Results of PPO with Multi-Branch Network.

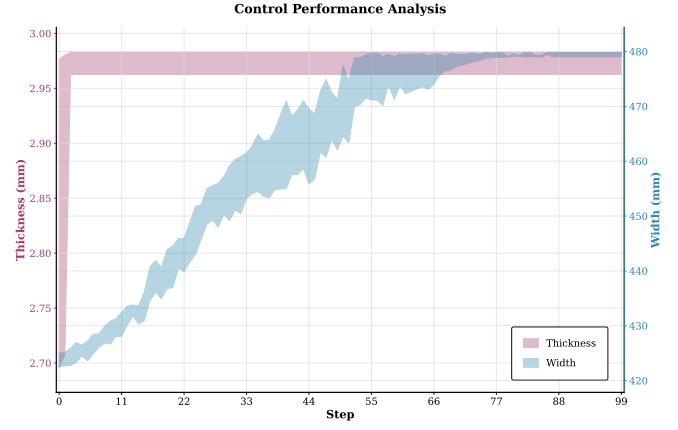


Fig. 8: Optimization Results of MPD-PPO with Differentiated Clipping Removed.

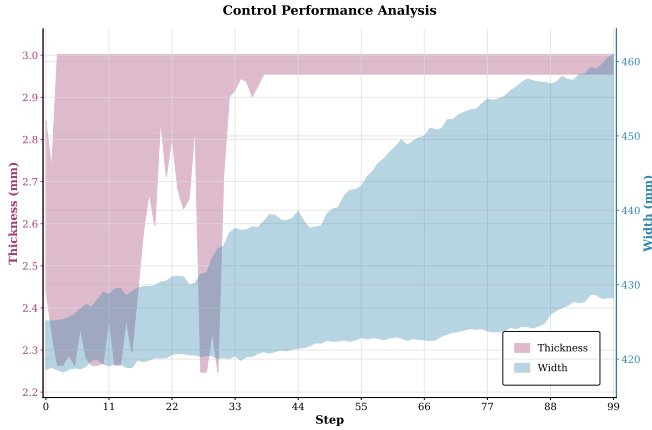


Fig. 7: Optimization Results of PPO Algorithm.

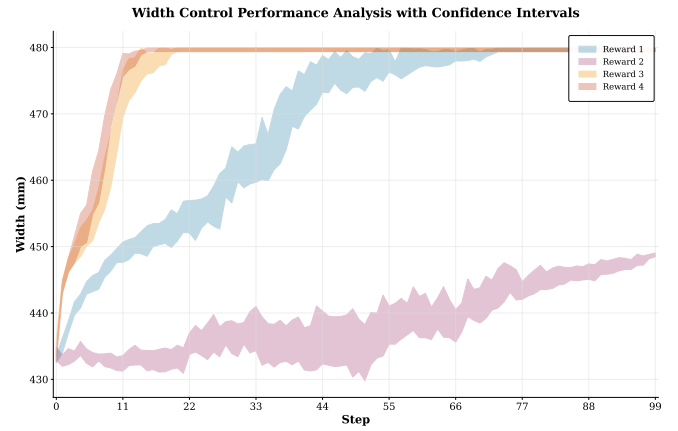


Fig. 9: The Impact of Reward-Function Modules on Optimization Results.

Compared to the standard MPD-PPO in Fig. 5, Fig. 8 displays the MPD-PPO without Differentiated Clipping results.

Experimental results confirm that although removing the differentiated clipping leads to significant performance degradation in film width optimization, the overall performance of our proposed method remains superior to the original PPO algorithm. Furthermore, since the MPD-PPO algorithm incorporates independent advantage estimation for each branch network, it demonstrates better optimization effectiveness than the PPO algorithm with branched networks from previous experiments, even without the differentiated clipping mechanism.

TABLE VII: Optimization Results Of Removing Differentiated Clipping.

Algorithm	Average Optimize Step
MPD-PPO	22
MPD-PPO Without Differentiated Clipping	87
PPO	100 (Failed)

3) *Impact of Reward-Function Modules on Optimization Performance:* To isolate the contribution of individual reward components, we performed a comparative analysis using width control as the test case, chosen due to the less pronounced

contrast in thickness scale. We derived all evaluated reward functions by systematically removing components from our proposed comprehensive function: Reward 1 uses only the Error Reward; Reward 2 combines Error and Progress Rewards; Reward 3 excludes the Steady-State Reward; Reward 4 is the complete function, integrating an action smoothness penalty with error and progress rewards to balance control accuracy and operational stability. The corresponding results are presented in Table VIII and Fig. 9. The experimental

TABLE VIII: The Impact of Reward-Function Modules on Optimization Results.

Algorithm	Average Optimize Step
Reward 1 (Use Only The Error Reward)	74
Reward 2 (Combines Error And Progress Reward)	100 (Failed)
Reward 3 (Excludes The Steady-State Reward)	22
Reward 4 (The Complete Reward Function)	16

results confirm that every component of the reward function contributes to the optimization of the width parameters, demonstrating the synergy of combining all the individual modules.

E. Experimental Validation on a Real-World Rubber Tyre Production Line

To rigorously assess the algorithm’s effectiveness under real-world industrial conditions, this study conducted testing in collaboration with MESNAC, on one of its operational production lines, the same industrial equipment as illustrated in Fig. 1. Process data were collected in real-time via PLC communication at a frequency of 0.2 ms intervals, directly from sensors and control systems. This *in-situ* validation strategy guarantees a high degree of fidelity to the actual production environments, thereby providing dependable evidence for assessing the algorithm’s performance. The experimental results are presented in Fig. 10 and Fig. 11. Experimental results from the production line demonstrate the robustness of the agent’s control strategy. In response to both positive and negative setpoint adjustments in width, the agent generated appropriate control actions that effectively guided the system state toward the target. The regulation process exhibited no significant overshoot, indicating favorable convergence characteristics.

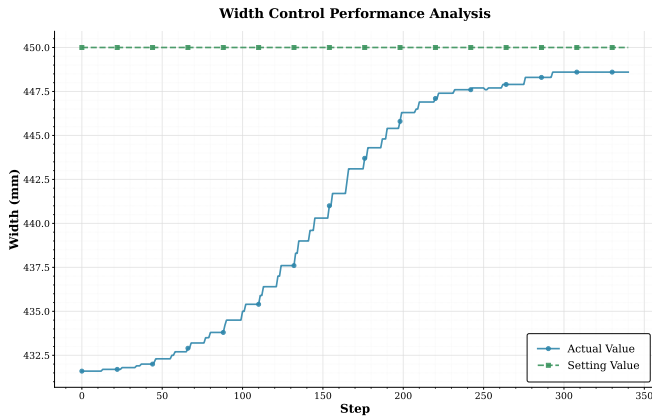


Fig. 10: Validation Results From A Real Rubber Tyre Production Line 1.

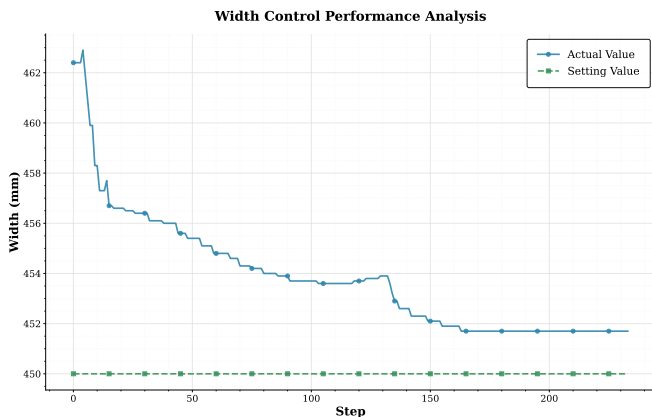


Fig. 11: Validation Results From A Real Rubber Tyre Production Line 2.

V. CONCLUSION

In this research, we propose a novel intelligent control framework that seamlessly integrates deep reinforcement

learning with predictive modeling to address multi-objective parameter optimization in complex industrial processes.

The proposed solution combines the predictive capabilities of LSTNet, which effectively captures both short-term fluctuations and long-term trends in complex time series data, with the Multi-path Differentiated Clipping Proximal Policy Optimization (MPD-PPO) algorithm. MPD-PPO employs a distributed policy architecture and an adaptive clipping mechanism to achieve differentiated and precise control. Furthermore, a composite reward function was designed to balance the competing objectives of accuracy, efficiency, and stability. Collectively, this research provides a scalable and adaptive solution for industrial autonomous optimization, demonstrating enhanced real-time performance and effective handling of multi-objective trade-offs and dynamic state processing. The methodology thus offers a promising pathway for advancing reinforcement learning applications in industrial informatics and control systems.

REFERENCES

- [1] M. Wollschlaeger, T. Sauter, and J. Jasperneite, “The future of industrial communication: Automation networks in the era of the internet of things and industry 4.0,” *IEEE industrial electronics magazine*, vol. 11, no. 1, pp. 17–27, 2017.
- [2] H. Jung and B. Lee, “Wireless power and bidirectional data transfer system for iot and mobile devices,” *IEEE Transactions on Industrial Electronics*, vol. 69, no. 11, pp. 11 832–11 836, 2021.
- [3] L. Ren, J. Dong, D. Huang, and J. Lu, “Digital twin robotic system with continuous learning for grasp detection in variable scenes,” *IEEE Transactions on Industrial Electronics*, vol. 71, no. 7, pp. 7653–7663, 2023.
- [4] J. Yu, C. Dou, and X. Li, “Mas-based energy management strategies for a hybrid energy generation system,” *IEEE Transactions on Industrial Electronics*, vol. 63, no. 6, pp. 3756–3764, 2016.
- [5] B. Hu and J. Li, “An edge computing framework for powertrain control system optimization of intelligent and connected vehicles based on curiosity-driven deep reinforcement learning,” *IEEE Transactions on Industrial Electronics*, vol. 68, no. 8, pp. 7652–7661, 2020.
- [6] J. Schulman, F. Wolski, P. Dhariwal, A. Radford, and O. Klimov, “Proximal policy optimization algorithms,” *arXiv preprint arXiv:1707.06347*, 2017.
- [7] S. Fujimoto, H. Hoof, and D. Meger, “Addressing function approximation error in actor-critic methods,” in *International conference on machine learning*, PMLR, 2018, pp. 1587–1596.
- [8] Z. Li, F. Liu, W. Yang, S. Peng, and J. Zhou, “A survey of convolutional neural networks: Analysis, applications, and prospects,” *IEEE transactions on neural networks and learning systems*, vol. 33, no. 12, pp. 6999–7019, 2021.
- [9] Y. LeCun, L. Bottou, Y. Bengio, and P. Haffner, “Gradient-based learning applied to document recognition,” *Proceedings of the IEEE*, vol. 86, no. 11, pp. 2278–2324, 2002.

- [10] A. Krizhevsky, I. Sutskever, and G. E. Hinton, “Imagenet classification with deep convolutional neural networks,” *Communications of the ACM*, vol. 60, no. 6, pp. 84–90, 2017.
- [11] K. He, X. Zhang, S. Ren, and J. Sun, “Deep residual learning for image recognition,” in *Proceedings of the IEEE conference on computer vision and pattern recognition*, 2016, pp. 770–778.
- [12] G. Huang, Z. Liu, L. Van Der Maaten, and K. Q. Weinberger, “Densely connected convolutional networks,” in *Proceedings of the IEEE conference on computer vision and pattern recognition*, 2017, pp. 4700–4708.
- [13] A. G. Howard et al., “Mobilenets: Efficient convolutional neural networks for mobile vision applications,” in *Proceedings of the IEEE conference on computer vision and pattern recognition*, 2017, pp. 7263–7271.
- [14] X. Zhang, X. Zhou, M. Lin, and J. Sun, “Shufflenet: An extremely efficient convolutional neural network for mobile devices,” in *Proceedings of the IEEE conference on computer vision and pattern recognition*, 2018, pp. 6848–6856.
- [15] K. Han et al., “A survey on vision transformer,” *IEEE transactions on pattern analysis and machine intelligence*, vol. 45, no. 1, pp. 87–110, 2022.
- [16] A. Graves, “Generating sequences with recurrent neural networks,” in *Proceedings of the 30th International Conference on Machine Learning*, vol. 28, 2013, pp. 1–9.
- [17] A. Graves, “Long short-term memory,” *Supervised sequence labelling with recurrent neural networks*, pp. 37–45, 2012.
- [18] J. Chung, C. Gulcehre, K. Cho, and Y. Bengio, “Gated feedback recurrent neural networks,” in *International conference on machine learning*, PMLR, 2015, pp. 2067–2075.
- [19] J. Fan, K. Zhang, Y. Huang, Y. Zhu, and B. Chen, “Parallel spatio-temporal attention-based tcn for multivariate time series prediction,” *Neural Computing and Applications*, vol. 35, no. 18, pp. 13 109–13 118, 2023.
- [20] A. Vaswani et al., “Attention is all you need,” in *Advances in neural information processing systems*, 2017, pp. 5998–6008.
- [21] G. Corso, H. Stark, S. Jegelka, T. Jaakkola, and R. Barzilay, “Graph neural networks,” *Nature Reviews Methods Primers*, vol. 4, no. 1, p. 17, 2024.
- [22] V. Mnih et al., “Human-level control through deep reinforcement learning,” *Nature*, vol. 518, no. 7540, pp. 529–533, 2015.
- [23] Z. Zhang, Z. Pan, and M. J. Kochenderfer, “Weighted double q-learning,” in *IJCAI*, 2017, pp. 3455–3461.
- [24] Z. Wang, T. Schaul, M. Hessel, H. Hasselt, M. Lanctot, and N. Freitas, “Dueling network architectures for deep reinforcement learning,” in *International conference on machine learning*, PMLR, 2016, pp. 1995–2003.
- [25] J. Schulman, S. Levine, P. Abbeel, M. Jordan, and P. Moritz, “Trust region policy optimization,” in *International conference on machine learning*, PMLR, 2015, pp. 1889–1897.
- [26] Y. Hou, L. Liu, Q. Wei, X. Xu, and C. Chen, “A novel ddpg method with prioritized experience replay,” in *2017 IEEE international conference on systems, man, and cybernetics (SMC)*, IEEE, 2017, pp. 316–321.
- [27] T. Haarnoja, A. Zhou, P. Abbeel, and S. Levine, “Soft actor-critic: Off-policy maximum entropy deep reinforcement learning with a stochastic actor,” in *International conference on machine learning*, Pmlr, 2018, pp. 1861–1870.
- [28] R. Gorsane, O. Mahjoub, R. J. de Kock, R. Dubb, S. Singh, and A. Pretorius, “Towards a standardised performance evaluation protocol for cooperative marl,” *Advances in Neural Information Processing Systems*, vol. 35, pp. 5510–5521, 2022.
- [29] P. E. Iturria-Rivera, M. Chenier, B. Herscovici, B. Kantarci, and M. Erol-Kantarci, “Channel selection for wi-fi 7 multi-link operation via optimistic-weighted vdn and parallel transfer reinforcement learning,” in *2023 IEEE 34th Annual International Symposium on Personal, Indoor and Mobile Radio Communications (PIMRC)*, IEEE, 2023, pp. 1–6.
- [30] T. Rashid, M. Samvelyan, C. S. De Witt, G. Farquhar, J. Foerster, and S. Whiteson, “Monotonic value function factorisation for deep multi-agent reinforcement learning,” *Journal of Machine Learning Research*, vol. 21, no. 178, pp. 1–51, 2020.
- [31] M. Janner, J. Fu, M. Zhang, and S. Levine, “When to trust your model: Model-based policy optimization,” in *Advances in Neural Information Processing Systems*, vol. 32, 2019, pp. 1–12.
- [32] A. Kumar, A. Zhou, G. Tucker, and S. Levine, “Conservative q-learning for offline reinforcement learning,” *Advances in neural information processing systems*, vol. 33, pp. 1179–1191, 2020.
- [33] E. Jacinto, F. Martinez, and F. Martinez, “Navigation of autonomous vehicles using reinforcement learning with generalized advantage estimation,” *International Journal of Advanced Computer Science and Applications*, vol. 14, no. 1, 2023.
- [34] S. Zhang, D. Zheng, X. Hu, and M. Yang, “Bidirectional long short-term memory networks for relation classification,” in *Proceedings of the 29th Pacific Asia conference on language, information and computation*, 2015, pp. 73–78.
- [35] H. Zhou et al., “Informer: Beyond efficient transformer for long sequence time-series forecasting,” in *Proceedings of the AAAI conference on artificial intelligence*, vol. 35, 2021, pp. 11 106–11 115.